HYDRODYNAMIC PUMPING OF A QUANTUM FERMI LIQUID IN A SEMICONDUCTOR HETEROSTRUCTURE

A thesis presented to

the faculty of

the College of Arts and Sciences of Ohio University

In partial fulfillment of the requirements

for the degree of

Master of Science

Deependra Kantha

November 2002

This thesis entitled

HYDRODYNAMIC PUMPING OF A QUANTUM FERMI LIQUID IN A SEMICONDUCTOR HETEROSTRUCTURE

By

Deependra Kantha

has been approved for

the Department of Physics and Astronomy

and the College of Arts and Sciences by

Jean J. Heremans

Assistant Professor of Physics and Astronomy

Leslie A. Flemming

Dean, College of Arts and Sciences

KANTHA, DEEPENDRA M.S. November 2002, Physics

Hydrodynamic Pumping of a Quantum Fermi Liquid in a Semiconductor Heterostructure (60 pp)

Director of Thesis: Jean J. Heremans

Hydrodynamic pumping effect in a two dimensional electron system is a new phenomenon. In this thesis, we are investigating hydrodynamic pumping in a GaAs/$Ga_{0.70}Al_{0.30}As$ heterostructure. The mesoscopic structure was written by electron beam lithography and photolithography. An electron beam was injected from one aperture into the Fermi sea of electrons. We observed that electrons were extracted from another aperture as the beam of electrons swept past that aperture at low magnetic fields. Both voltage and current measurements were performed to confirm the results. The results show that the hydrodynamic pumping force is linear in terms of carrier injection from the aperture.

The theoretical background is provided by Dr. A.O. Govorov. The theory treats a Boltzmann transport equation in the relaxation time approximation. When electrons are injected from an aperture, positive potential develops in the nearby region because non-equilibrium electron density will be less than the equilibrium density of electrons and increases the positive charge density. It generates an attractive pumping force. This phenomenon is qualitatively different from the Bernoulli effect in classical liquids.

Approved: Jean J. Heremans

Assistant Professor of Physics and Astronomy

Acknowledgments

I would like to express my sincere gratitude to my advisor- Dr. Jean J. Heremans for his guidance and support. He is a knowledgeable mentor and a trustworthy friend.

I acknowledge the faculty and staff of the Department of Physics and Astronomy. Their help made it possible for me to complete my study here.

I need to acknowledge Dr. A. O. Govorov for providing theoretical explanation for the experiment.

I wish to thank Dr. Victoria Soghomonian for her guidance and encouragement. I also wish to acknowledge my friends Daniel Asare and John A. Peters for their kind support in my work.

I wish to thank my wife, Amrita for encouraging and supporting me in these couple of years.

I would like to thank M. Shayegan (Princeton University) for the high mobility GaAs/AlGaAs heterostructure.

Financial support from Ohio University is greatly appreciated as well as the support under Dr. Heremans's grant NSF DMR-0094055.

Table of Contents

List of Figures

List of Equations

CHAPTER 1

Introduction

The Bernoulli effect in classical liquid states that

Pressure (P), kinetic energy per unit volume (½ ρv^2) and potential energy per unit volume (ρgh) is constant along the streamline. [1]

For horizontal terminals,

$$(P_1 - P_2) = \frac{1}{2} \rho (v_2^2 - v_1^2) \qquad \text{-------------(1.1)}$$

where,

P_1 and P_2 are the pressures at two terminals and v_1 and v_2 are the velocities at respective terminals

$$\text{or, } \Delta P = \frac{1}{2} \rho v^2$$

When a fluid flows through a tube of uniform cross section, the fluid exerts a force on the solid surface. One component of the force is due to stationary state of fluid and another component is due to motion of fluid [2]. This kinetic component of the force can be calculated as

$$F = \frac{1}{2} \rho v^2 A f \qquad \text{--------------------(1.2)}$$

Where,

F is kinetic component of force

A is cross section area of tube

f is friction factor

The force in terms of change in pressure

$$F = \Delta P.\ A$$

$$\therefore\ \Delta P = \tfrac{1}{2}\, \rho\, v^2\, f \qquad \text{----------------(1.3)}$$

The friction factor for laminar flow in long tube can be defined in terms of the Reylonds number as

$$f = \frac{16}{R_e}$$

and the Reylonds number is

$$R_e = \frac{D\, v\, \rho}{\mu}$$

where,

D is diameter of tube

v is average velocity

μ is coefficient of viscosity

$$\text{So,}\quad \Delta P = \frac{1}{2}\rho\, v^2\, \frac{16\,\mu}{D\, v\, \rho}$$

$$= 8\,\frac{\mu}{D}\, v \qquad \text{--------------(1.4)}$$

From above equation (1.4), we see that the change in pressure is directly proportional to velocity when we consider viscous flow of liquid in laminar flow of region.

In this thesis, we tried to see the Bernoulli's effect in the context of charge flow in a two dimensional electron system (2DES) at very low temperature.

In a GaAs/AlGaAs heterostructure, electrons accumulate at the corners of the band bending. Remote doping of GaAs helps to achieve high electron concentration in the channel while retaining high mobility. The 2DES is buried 680Å from the top surface.

The device geometry [3, 4] was written by electron beam lithography as shown in figure 1.1. The scale of the geometry was determined in such a way that the momentum relaxation mean free path, l_{μ} and the electron-electron interaction path, l_{ee} were larger than the opening of the aperture and than the distance between the apertures [5, 6, 7].

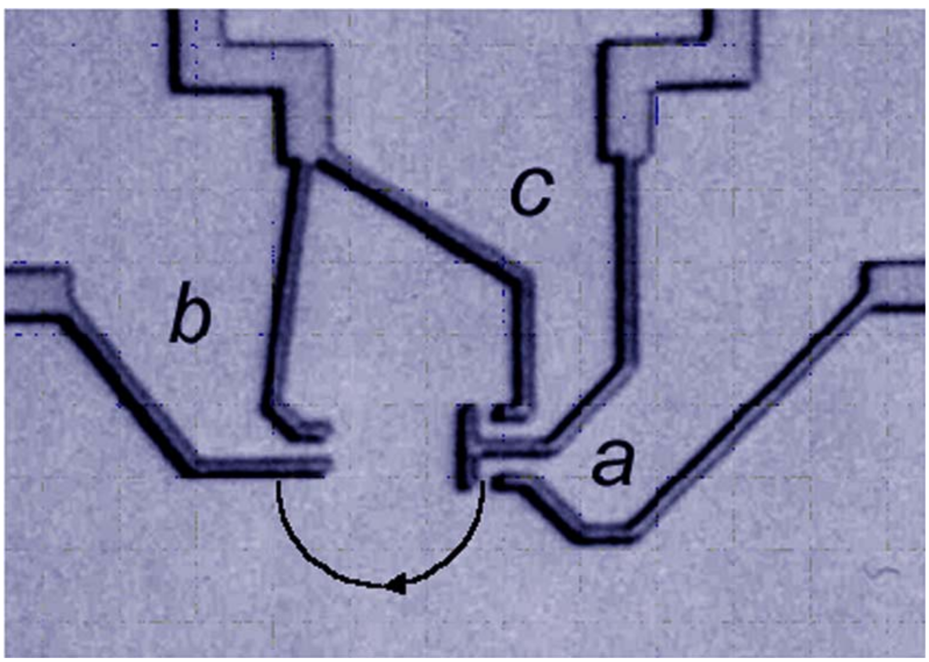

Figure 1.1: The device geometry on a two-dimensional electron system, in which the pumping effect is observed. The dark lines act as electrostatic barriers for charge carriers. The electron beam is injected from aperture **a** and sweeps past aperture **b** under the external magnetic field. The direction of the induced pumping effect from aperture **b** is indicated by the dashed arrow.

At low temperatures, the electron-electron interaction is very low. The electron-electron interaction path l_{ee} will be comparatively longer than the momentum relaxation mean free path l_{μ}. So the two dimensional electron system can be treated as a dilute classical liquid.

A hydrodynamic effect is observed when the electron beam sweeps past an aperture. As the beam of electrons sweeps past an aperture, the beam will extract electrons from that aperture. This extraction of electrons depends linearly on the injection current of electrons. We also investigated the temperature dependence of the hydrodynamic pumping force. The results shows that the pumping force is not so strong at higher temperatures where the electron-electron interaction path is smaller than the momentum relaxation mean free path.

A ballistic beam of electrons is injected from aperture **a** (figure 1.1) and is forced to sweep past aperture **b** by an external perpendicular magnetic field. The voltage is measured at aperture **b** as a function of the magnetic field as shown in figure 1.2. In the figure 1.2, the negative peak is observed at B = 0.027 T (temperature T = 1.3 K) and the negative voltage at low magnetic fields indicates the carrier extraction from aperture **b**.

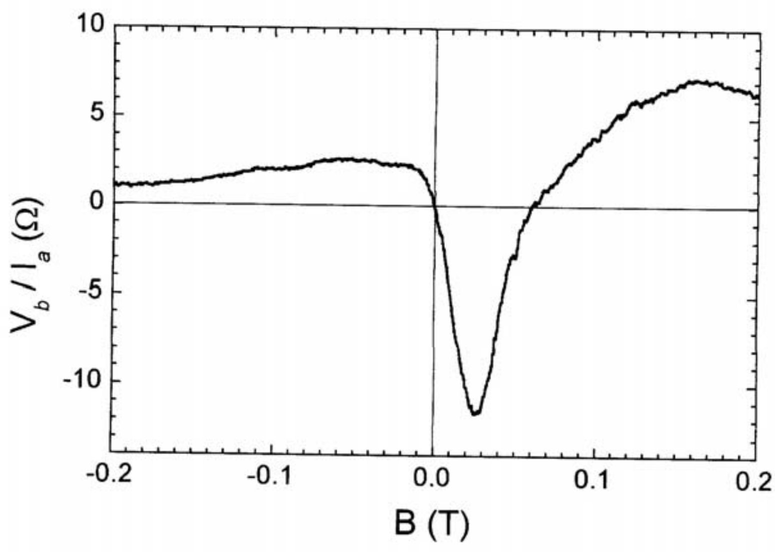

Figure 1.2: The voltage V_b measured at aperture **b** with respect to ground, as function of the applied perpendicular magnetic field B at temperature T= 1.3 K. A negative V_b signifies that potentials at **b** and at **a** are of opposite signs, and indicates carrier extraction from **b**.

One experiment was performed to verify linearity between the injection current and the extraction current. This linearity is qualitatively different from the Bernoulli effect in classical liquids where the pumping force is non-linear and quadratic.

A theoretical explanation was provided by Dr. A. O. Govorov. The Boltzmann transport equation including an electron-electron collision integral was solved within the relaxation time approximation. Applying boundary conditions at the injection aperture gives a non-equilibrium carrier density distribution. The non-equilibrium electron density, δn, is defined as

$$\delta n = n - n_0$$

where,

n is the density of electrons

n_0 is the equilibrium density of electrons.

The non-equilibrium electron density becomes negative in the nearby regions of the aperture leading to an attractive pumping force. This pumping force is attributed to a weak electron-electron interaction in the Fermi gas at low temperatures.

CHAPTER 2

SAMPLE FABRICATION

2.1 Heterostructure

A piece of 5 mm x 4 mm GaAs/$Ga_{0.70}Al_{0.30}As$ wafer was placed in trichloroethylene for 3 minutes. Subsequently it was also cleaned for 3 minutes each in acetone and isopropanol. For better cleaning, the wafer piece in these chemicals was placed in an ultrasonic cleaner.

The GaAs/GaAlAs triangular well heterostructure contains a high mobility 2DES, 680 Å below the surface. It is grown by molecular beam epitaxy on an undoped (100) GaAs substrate. A buffer layer is deposited on the substrate. Then a layer of GaAs of thickness 10,000 Å is grown on it, followed by a 20 Å layer of AlAs. After that, a layer of $Al_{0.30}Ga_{0.70}As$ of thickness 420 Å is grown on top of the AlAs. There are also ten layers of δ-Si separated by $Al_{0.30}Ga_{0.70}As$ of thickness 20 Å. The topmost layer is GaAs of thickness 60 Å. The layer profile is given in figure 2.1.

1	→	GaAs layer of thickness 60Å
2	→	10 layers of δ-Si of thickness 20 Å each
3	→	$Ga_{0.70}Al_{0.30}As$ layer of thickness 420Å
4	→	AlAs layer of thickness 20 Å
5	→	GaAs layer of thickness 10,000Å
6	→	Buffer layer
7	→	GaAs (100) substrate

Figure 2.1: Sample GaAs/GaAlAs grown on GaAs(100) substrate (not to scale).

2.2 Photolithography

Photolithography is the process of transferring geometric patterns and shapes to the surface of a semiconductor wafer by exposing the surface to high intensity ultraviolet beam [8]. The steps involved in the photolithographic process are wafer cleaning, deposition of a photoresist on the sample, soft baking, exposure and development.

The sample was glued on an 18 mm x18 mm glass plate. It was spun with a drop of photoresist (AZ5206E) on the surface for 40 seconds at a speed of 3500 revolutions per minute. The sample was heated at 90ºC for 30 minutes in a convection oven before performing the photolithography. The sample was aligned with a photo mask in the machine (a photo mask is a square glass plate with a pattern emulsion on one side). The mask was aligned with the sample so that the pattern could be transferred onto the sample surface. Once aligned accurately, the photoresist was exposed by a high intensity ultraviolet beam for 7 seconds. The exposed sample was developed in a 351-H_2O chemical developer for 25 seconds. Figure 2.2 is the picture of the photomask pattern transferred onto the sample. On the left hand side of the pattern is a Hall bar with a length of 300 μm and a width of 150 μm. The dark lines are mesa to connect with device geometry.

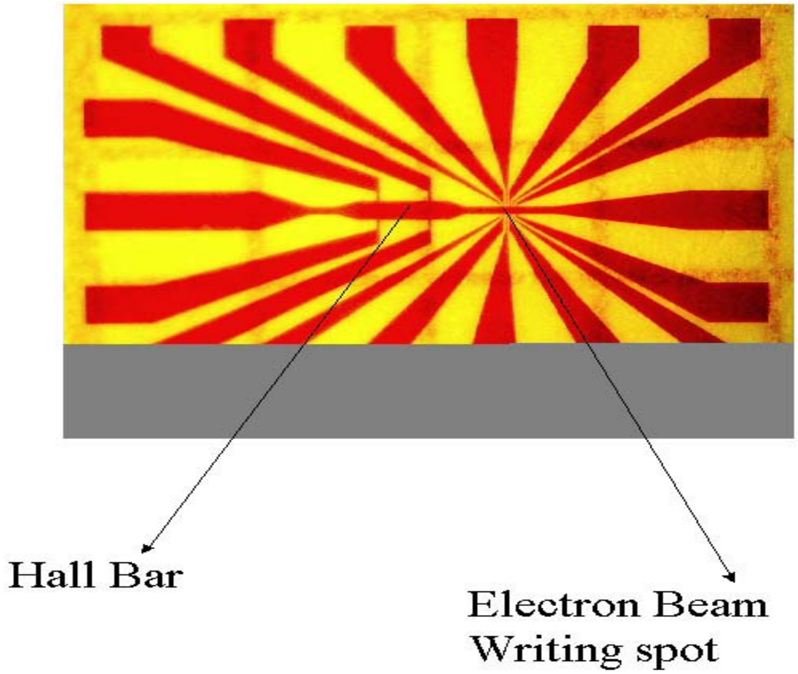

Figure 2.2: Picture of photomask

2.3 Electron Beam Lithography

Electron beam lithography is a technique used for writing the extremely fine patterns that are applicable in nanometer-scale scientific research and in modern electronics industry for creating integrated circuits by using a scanning electron microscope. A beam of electrons is scanned on the sample covered with an electron beam resist and the beam deposits energy in the desired pattern [9].

The sample was attached to a gold plated glass slide to keep the sample electrically neutral during the electron-beam writing process. The sample was covered with 2 drops of an electron beam resist; a 3% PMMA(polymethyl methacrylate). The common polymer PMMA is an excellent electron beam resist. It was then spun at a speed of 7400 revolutions per minute for 40 seconds. To harden the PMMA layer, we baked the sample at 160ºC for four hours.

The main parameters for writing electron beam pattern were set as follows:

Beam current: 7.5 pA

Magnification: 750

Area dose: 430 μC/cm^2

Once the pattern was written, it was developed in a 3:1 ratio of an IPA:MIBK (Isopropanol: Methyl Iso-Butyl Ketone) solution for 70 seconds. It was then rinsed in isopropanol for a few seconds . The opening of the apertures **a**, **b** and **c** is 0.6 μm. When the pattern was etched, there was a vertical as well as a horizontal depletion. Due to the side depletion, the conducting opening was estimated to be around 0.4 μm. Figure 2.3 shows the pattern after developing. The dark lines denote wet etched regions, depleted of carriers. The thickness of dark lines is 0.3 μm. They act as electrostatic barriers for charge carriers being injected or extracted from the apertures **a**, **b** or **c**. The distance between apertures **a** and **b** is 5.6 μm.

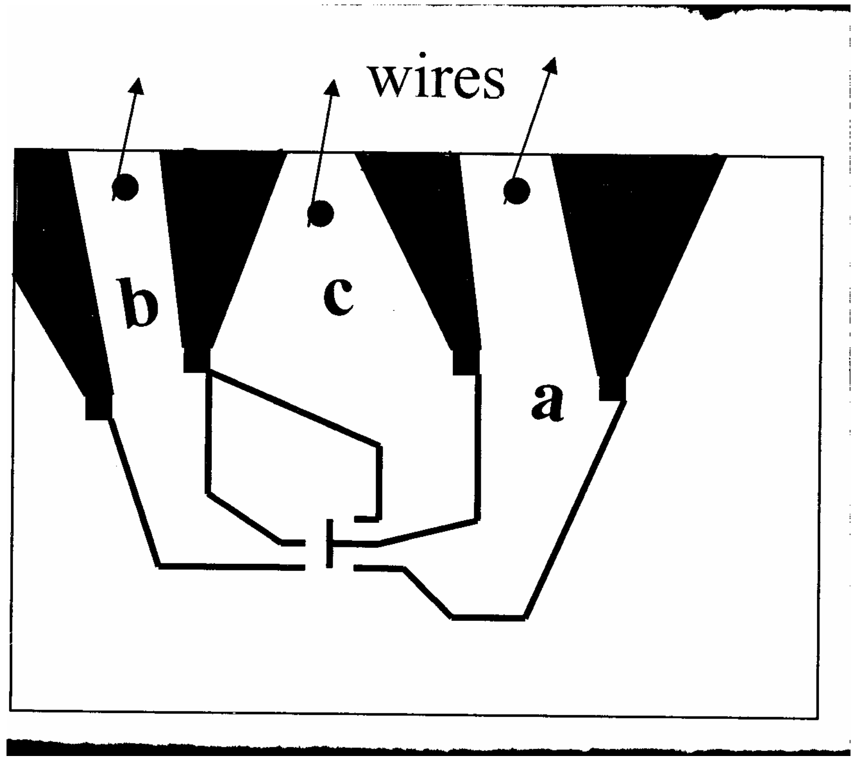

Figure 2.3: The electron-beam pattern after developing. Dark lines are electrostatic barrier for electrons. Charge carriers are injected or extracted from apertures **a**, **b** or **c**.

2.4 Etching

After the electron beam lithography the sample was baked at 90°C for 15 minutes to harden the PMMA. It was then etched in an etchant solution of H_2SO_4:H_2O_2:H_2O in the ratio 1:8:40 for 10 seconds. We rinsed it in hot water for 2-3 minutes. The sample was placed in acetone to get rid of PMMA and other impurities.

2.5 Annealing

With the etching process complete, we put very small contacts of In-Sn to connect the experimental wires. These contacts are on the surface of GaAs. We annealed the sample to form ohmic contacts with the two dimensional electron system. The process involved keeping the sample in the annealing box and flushing the box with N_2-H_2 gas during the whole process. The sample was heated to 120°C for 2 minutes to evaporate water. In the next stage, it was heated to 170°C for 1 minute to melt the indium. The sample was further heated to 425°C for 10 minutes to form the ohmic contact.

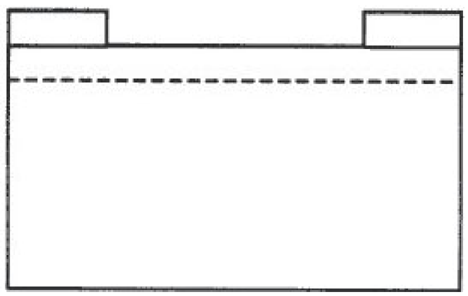

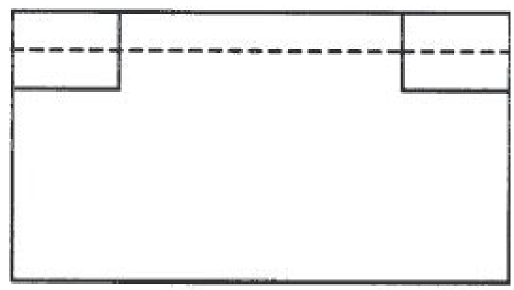

Figure 2.4(a) Figure 2.4(b)

In figure (a), In-Sn contacts are on the surface before annealing. In figure(b), contacts are annealed in the 2DES.

2.6 Evaporation

After annealing a gate of Cr/Au was evaporated on top of the sample. To avoid a shorted gate, we covered the contacts with photoresist and the sample piece was heated at 90°C for 40 minutes to harden the resist. The sample was then placed in the vacuum chamber of an evaporator. A chromium layer of thickness 206 Å was first deposited on the whole surface. This deposition was to help the gold stick better on the surface of the sample. Then, a gold layer of thickness 620 Å was deposited on top of the chromium.

After evaporation the sample was placed in acetone for lift-off to get rid of the photoresist paint on the contacts. The sample was then mounted on a cold-head probe.

2.7 Cooling Process

For low temperature measurements, the sample had to be cooled to ~ 0.3 K. First of all, the dewar was cooled to 77 K with liquid nitrogen. The dewar temperature was indicated by a carbon resistance thermometer on top of the magnet. The dewar was further cooled down to 4.2 K with liquid ^{4}He. The magnet inside the dewar was then at a superconducting stage. The dewar was almost filled with liquid ^{4}He. We can cool down the sample either to 1.2 K or to 0.33 K.

To cool down the sample to 1.2 K, the central can of the dewar was pumped to a very low pressure (almost vacuum). The liquid ^{4}He was transferred to the central can of the dewar. Because of the very low pressure, liquid ^{4}He boils at about 1.2 K. The probe was filled with a ^{4}He exchange gas at low pressure. The probe was then inserted into the central can of the dewar and heat exchange took place. The temperature of the sample went down to 1.2 K.

To cool down the sample to 0.33 K, we used a ^{3}He cooling system as well. The probe was kept at a high vacuum and was inserted in the main dewar. The liquid ^{3}He was pumped into the probe and it condensed. At this point, the sample was in the ^{3}He liquid bath. After pumping on the ^{3}He liquid, the lowest temperature achieved was 0.33 K. A cernox resistance thermometer was used to measure the low temperatures.

CHAPTER 3

MEASUREMENT

3.1 Lock-in Technique

All measurements were done in four-contact mode. One terminal was assumed to be ground. The four contacts were associated with the Hall bar. Two contacts were for the injection of current through an aperture; the other two contacts were used for current or voltage measurements at another aperture. The experimental wires were connected to a set of lock-in amplifiers, resistances and dc sources as required. The measurements involved very small signals of the order of nanoamperes and microvolts. These types of signals were buried under noise from AC power supplies, sparks of switch or radio noise. Lock-in amplifiers amplify these small signals and eliminate other disturbances [10]. The small signals can be extracted by reducing signal band-widths to a satisfactory noise level. The basic building block of a lock-in amplifier is a phase sensitive detector. For measurements, we used a low pass filter to pass dc and low frequency ac signals and block high frequency signals.

3.2 Shubnikov-de Haas Effect:

The resistivity of a 2DES is approximately constant at low magnetic fields but develops strong oscillations with zeros at higher fields and lower temperatures. This is the Shubnikov-de Haas effect [11]. The effect is caused by the fact that a magnetic field applied perpendicular to a two dimensional electron system causes the formation of discrete quantized orbits called Landau levels. The Landau levels increase linearly in energy with increasing magnetic field. This linearity arises from the fact that the cyclotron resonance frequency, $\omega_c = eB/m^*$, where h is Planck's constant, n is the density of electron in two dimensions and m* is the effective mass of an electron.

Longitudinal conduction occurs at the Fermi level and therefore disappears when the density of states goes to zero at B = hn/eν, where ν is the number of exactly full Landau levels [11]. The Fermi level E_F moves with the density of states to keep the number of electrons constant.

The position of the Fermi level E_F has a qualitative effect on the electronic behavior of a 2DES. If E_F lies within a Landau level, the density of states at the Fermi level is high. If E_F lies within a gap, a small change in energy has no effect at all on the density of the 2DES because the density of states at the Fermi level is zero.

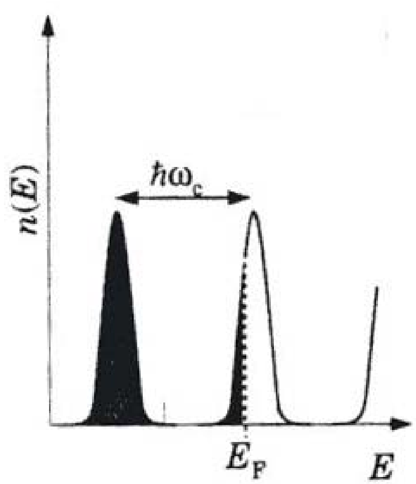

Figure 3.1(a)

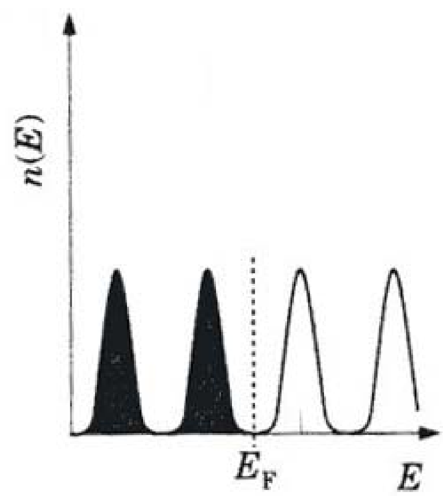

Figure3.1(b)

Figure 3.1: Occupation of Landau Levels in a magnetic field

As the magnetic field is increased, these Landau levels will pass through the Fermi level causing oscillations in the conductivity.

From Shubnikov-de Haas oscillations, we can calculate the surface electron density. By Fourier analysis of the oscillation graph, the frequency of oscillation is determined.

By knowing the longitudinal resistance and the electron density, we can analyze the data further by calculating the mobility and the momentum relaxation mean free path.

3.3 Hall Effect

When a current J_x is applied across the specimen in the presence of a magnetic field B, an electric field E_y is developed in the direction of $\mathbf{J_x} \times \mathbf{B}$. This is known as the Hall effect [12].

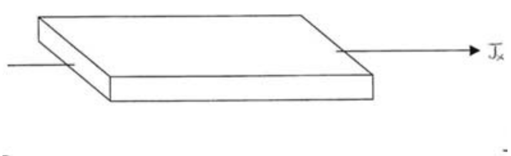

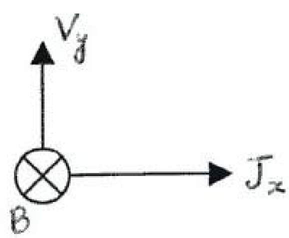

Figure 3.2(a) Figure 3.2(b)

Figure 3.2(a): The standard geometry of a specimen for the Hall effect. In figure (b), current is applied along the x-axis, magnetic field is applied along the z-axis, and hall voltage is measured along the y-axis.

The Hall coefficient R_H is defined as [12]

$$R_H = \frac{E_y}{J_x B} \qquad \text{-------------------------------(3.1)}$$

The Hall resistance in a two dimensional system is given by

$$\rho_h = BR_h \qquad \text{-------------------------------(3.2)}$$

$$\text{or,} \quad R_h = -\frac{\rho_h}{B}$$

Where,

B = Magnetic field

R_h = Hall coefficient in two dimension system and is defined as

$$R_h = -\frac{1}{ne} \qquad \text{------------------------------(3.3)}$$

Here,

e = charge of an electron

n = Number of electron per unit area

$$\text{or,} \quad \mathrm{n} = -\frac{1}{\mathrm{e\,R_h}} \qquad \text{-----------------------------(3.4)}$$

CHAPTER 4

RESULTS AND ANALYSIS

4.1 Results at temperature 0.4 K

We measured the electron density, the mobility and the mean free path from both Shubnikov-de Haas oscillations and the Hall resistance. A very small excitation current of 100 nA was used to avoid electron heating.

First, measurements were taken at a temperature of 0.4 K with a zero gate voltage. In figure 4.1, the longitudinal resistance was plotted as a function of inverse magnetic field. The magnetic field was applied perpendicular to the surface. The graph shown is the Shubnikov-de Haas oscillations.

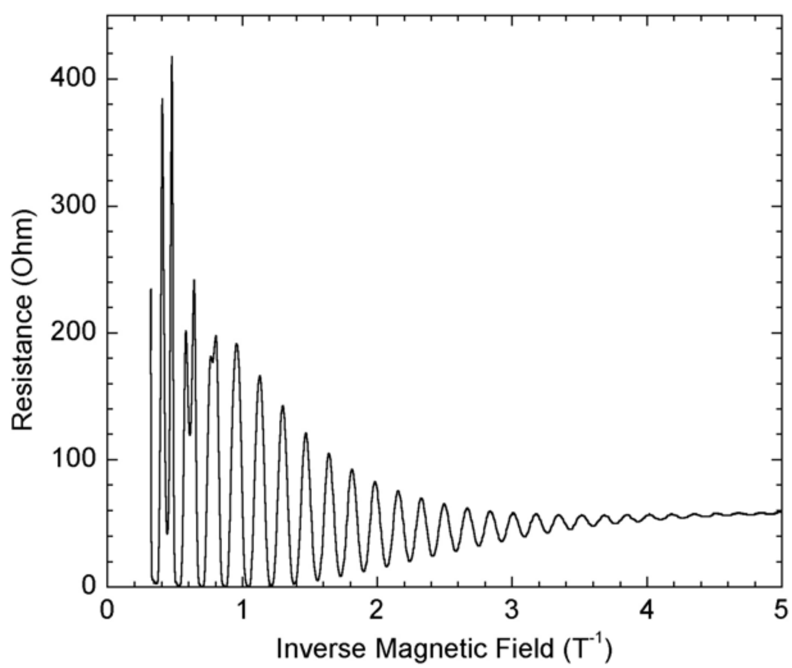

Figure 4.1: Longitudinal resistance R_L versus inverse of the applied perpendicular magnetic field B shows Shubnikov-de Haas oscillations at temperature 0.4 K and a zero gate voltage.

The frequency of oscillation can be obtained by Fourier analysis of the data. The simple way to calculate the electron density is as follows:

For an inverse magnetic field of $1T^{-1}$, the number of periods of oscillations is 6. So,

$$\text{Period of oscillations, T} = \frac{\text{Inverse Magnetic Field}}{\text{No. of Periods}}$$

$$= \frac{1}{6}\ T^{-1}$$

$$\text{Frequency, } f = \frac{1}{T}$$

$$= 6 \text{ Tesla}$$

$$\therefore \text{ Density of electrons, } n = 4.84 \times 10^{10}\ cm^{-2}\ T^{-1} \times f$$

$$= 4.84 \times 10^{10} \times 6\ cm^{-2}$$

$$= 2.90 \times 10^{11}\ cm^{-2}$$

$$= 2.90 \times 10^{15}\ m^{-2}$$

The alternate method to calculate electron density is from the Hall coefficient. In figure 4.2, the transverse resistance was plotted as a function of the applied perpendicular magnetic field. The transverse resistance was obtained by dividing the transverse voltage by the applied current. A very small excitation current of 100 nA was used to avoid electron heating. The slope of the curve gives the Hall coefficient.

Now, Hall coefficient R_h = slope of curve

$$= 2273.33\ \Omega/T$$

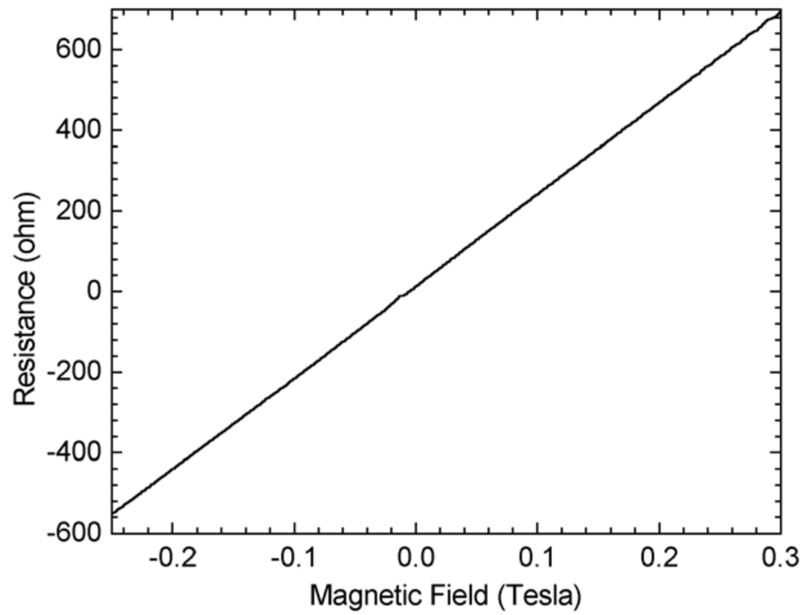

Figure 4.2: The transverse Resistance R as a function of applied perpendicular magnetic field at a temperature of 0.4 K and a zero gate voltage.

From equation (3.4),

$$\text{Density of Electrons, } n = \frac{1}{e R_h}$$

$$= \frac{1}{1.6 \times 10^{-19} \times 2273.33} \ m^{-2}$$

$$= 2.75 \times 10^{15} \ m^{-2}$$

The gate voltage was increased to increase the areal charge density. Figure 4.3 shows the Shubnikov-de Haas effect when the longitudinal voltage was measured and plotted as a function of the inverse applied magnetic field. The sample was still kept at T = 0.4 K in liquid ^{3}He and the gate voltage was V_g= 0.3 V. The magnetic field sweeping rate was 0.1 T/min.

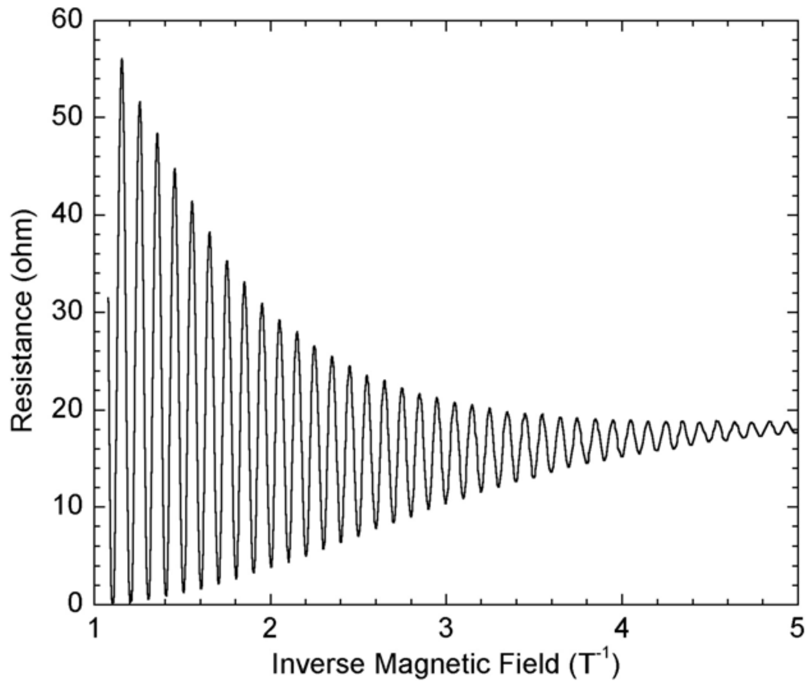

Figure 4.3: Longitudinal resistance R_L versus applied perpendicular magnetic field B_{ext} shows Shubnikov-de Haas oscillations at a temperature of 0.4 K and 0.3 V gate voltage in a uniform magnetic field sweeping at a rate of 0.1 T/min.

Now,

Number of periods = 10

Inverse magnetic Field = 1 T^{-1}

$$\text{Period of oscillations T} = \frac{\text{Inverse Magnetic Field}}{\text{No. of Periods}} = \frac{1}{10}\ T^{-1}$$

$$\text{Frequency } f = \frac{1}{T} = 10 \text{ T}$$

$$\therefore \text{ Electron Density n} = 4.84 \times 10^{10}\ cm^{-2}\ T^{-1} \times f$$

$$= 4.84 \times 10^{11}\ cm^{-2}$$

$$= 4.84 \times 10^{15}\ m^{-2}$$

Next, we calculated the electron density, the mobility, the momentum relaxation mean free path at a temperature of 0.4 K and gate voltage of 0.3 V from the Hall coefficient. In figure 4.4, the transverse resistance was plotted as a function of the applied perpendicular magnetic field.

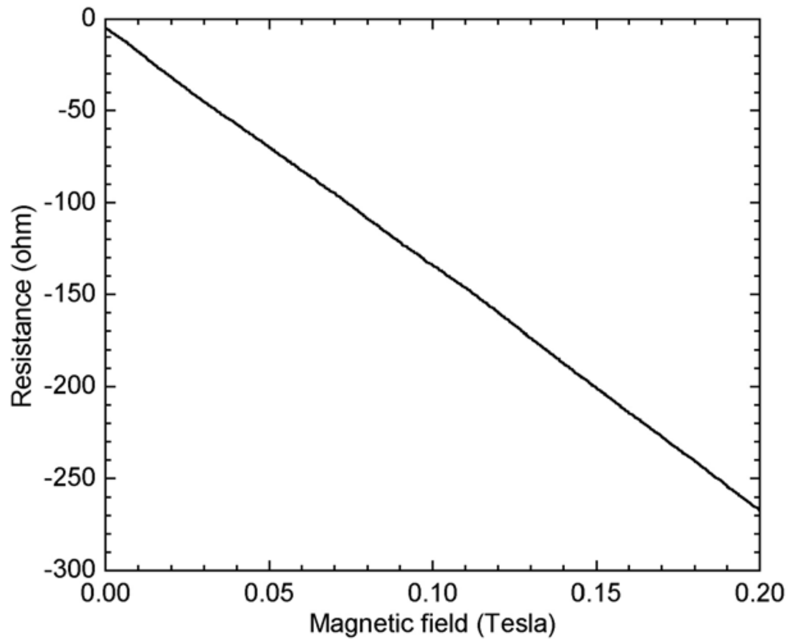

Figure 4.4: The transverse Resistance R as a function of the applied perpendicular magnetic field at a temperature of 0.4 K and 0.3 V gate voltage. Magnetic field is decreased at 0.02 T/min.

From the graph,

$$\text{Hall coefficient} = \text{slope of curve Resistance vs. magnetic field}$$

$$= -1350.06\ \Omega/\mathrm{T}$$

From equation (3.4),

$$\text{Density of Electrons } n = -\frac{1}{e R_h}$$

$$= \frac{1}{1.6\times10^{-19}\times1350.06}\ \mathrm{m}^{-2}$$

$$= 4.63 \times 10^{15}\ \mathrm{m}^{-2}$$

To calculate the mobility and the mean free path, we proceed as follows:

Longitudinal voltage $V = 1.515 \times 10^{-6}$ V

Applied current $I = 100 \times 10^{-9}$ A

Resistance $R = \frac{V}{I}$

$$= \frac{1.515\times10^{-6}}{100\times10^{-9}}\ \Omega$$

$$= 15.15\ \Omega$$

We know that the resistivity of a Hall bar in two dimensions can be written as

$$\rho = \frac{W}{L}R \qquad \text{---------------------------(4.1)}$$

where,

W = width of Hall bar

L = Length of Hall bar

R = Longitudinal Resistance

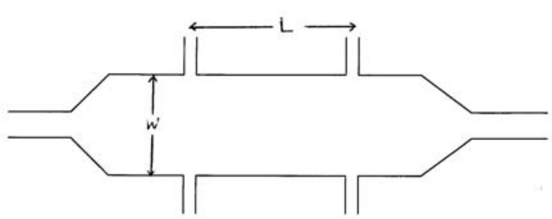

Figure 4.5: Hall bar used to calculate the Hall coefficient. The length is 300 μm and the width is 150 μm.

In our case,

W= 150 μm

L = 300 μm

$$\therefore \quad \rho = \frac{150}{300} \times 15.15 = 7.57\ \Omega$$

The electrical conductivity is defined by the relation

$$\sigma = ne\mu \qquad \text{------------------------------(4.2)}$$

where,

σ is electrical conductivity

μ is mobility

$$\text{or, } \frac{1}{\rho} = ne\mu$$

$$\text{or, } \mu = \frac{1}{ne\rho} \qquad \text{---------------------------------(4.3)}$$

$$= \frac{1}{4.63 \times 10^{15} \times 1.60 \times 10^{-19} \times 7.57}\ \mathrm{m^2/Vs}$$

$$= 178\ \mathrm{m^2/Vs}$$

It helps us to characterize the sample as having high electron density and high mobility.

The momentum relaxation mean free path is given by

$$l_\mu = \frac{\hbar}{e}\sqrt{2\pi}\,\mu\sqrt{n} \qquad \text{----------------------------(4.4)}$$

where $\hbar$ is reduced Planck's constant.

$$= \frac{1.05 \times 10^{-34} \times \sqrt{2 \times 3.14} \times 178 \times \sqrt{4.63 \times 10^{15}}}{1.60 \times 10^{-19}} \text{ m}$$

$= 19.9 \times 10^{-6}$ m

$= 20$ µm

Other parameters such as the Fermi energy and the Fermi velocity are also calculated.

The Fermi wave vector K_F in a two dimensional system in terms of the density of electrons **n** is

$$K_F = (2\pi \mathbf{n})^{1/2} \qquad \text{-------------------------(4.5)}$$

$= (2 \times 3.14 \times 4.63 \times 10^{15})^{1/2}$ m^{-1}

$= 1.70 \times 10^{8}$ m^{-1}

The Fermi energy of the system is

$$E_F = \frac{\hbar^2 K_F^2}{2m^*} \qquad \text{----------------------------(4.6)}$$

where m^* is the effective mass of electron

$$E_F = \frac{(1.05 \times 10^{-34})^2 \times (1.70 \times 10^{8})^2}{2 \times 0.067 \times 9.11 \times 10^{-31}} \text{ J}$$

$= 2.62 \times 10^{-21}$ J

$= 16.41$ meV

The Fermi wavelength is

$$\lambda_F = \frac{2\pi}{K_F} \qquad \text{--------------------------(4.7)}$$

$$= \frac{2 \times 3.14}{1.70 \times 10^{8}} \text{ m}$$

$= 3.69 \times 10^{-8}$ m

The Fermi velocity V_F is calculated from the relation

$$m^* V_F = \hbar K_F \qquad \text{---------------------(4.8)}$$

$$\text{or, } V_F = \frac{\hbar K_F}{m^*}$$

$$= \frac{1.05 \times 10^{-34} \times 1.71 \times 10^{8}}{0.067 \times 9.11 \times 10^{-31}} \text{ m/s}$$

$$= 2.93 \times 10^{4} \text{ m/s}$$

We set up the measurement system to observe the hydrodynamic pumping effect. In figure 4.6, the voltage was measured at the aperture **b** (refer to figure 1.1) with respect to a faraway contact, as a function of the applied perpendicular magnetic field and normalized to the current injected from the aperture **a**. The gate voltage and temperature were 0.3 V and 0.4 K respectively. The magnetic field was increased at 0.1 T/min.

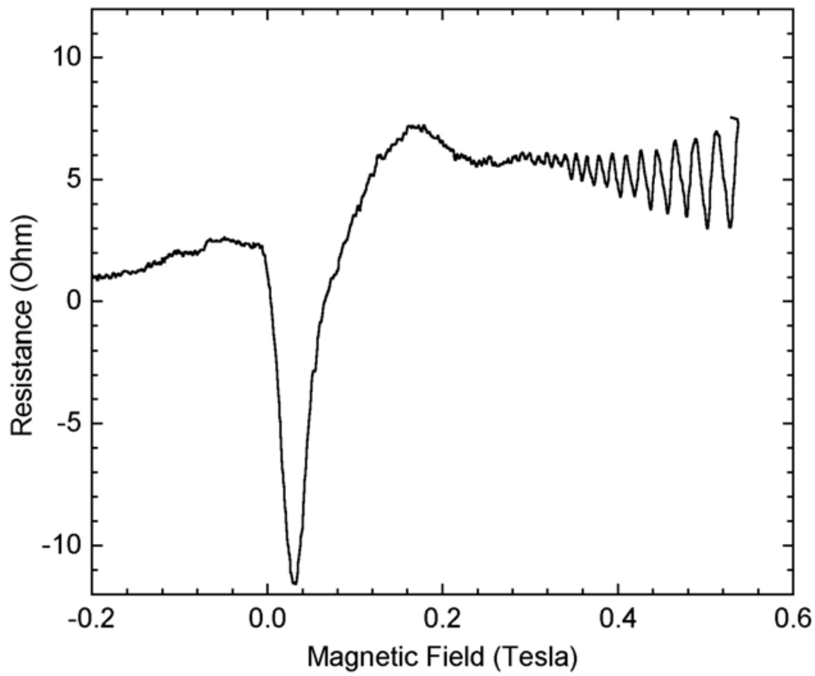

Figure 4.6: The voltage measured at aperture **b** with respect to a faraway contact, as a function of the applied perpendicular magnetic field and normalized to the current injected from aperture **a**. The gate voltage and temperature are 0.3 V and 0.4 K respectively. Magnetic Field is increased at 0.1 T/min.

The data was obtained by using a low frequency lock-in amplifier. A negative resistance indicates that the potential in contact **a** is of opposite polarity to that in contact **b**, with respect to a faraway contact. The negative peak was observed at the field B = 0.027 T. At this point, the radius of cyclotron orbit is given by

$$r = \frac{\hbar K_F}{Be} \qquad \text{------------------------(4.9)}$$

$$= \frac{1.05\times 10^{-34}\times 1.71\times 10^{8}}{0.027\times 9.10\times 10^{-31}}\ \text{m}$$

$$= 4.15 \times 10^{-6}\ \text{m}$$

$$= 4.15\ \mu\text{m}$$

The diameter of the cyclotron orbit is 8.3 μm.

The hydrodynamic pumping phenomenon can be explained by a schematic diagram shown in figure 4.7. A current I_i is injected from aperture **a** and the detector regions **b** or **c** is treated as a closed reservoir. At low magnetic field, the electrons will sweep past an aperture **b** or **c** and in the vicinity of the beam of electrons, the non-equilibrium electron density, δn, becomes less than the equilibrium density of electrons. This causes electrons to be extracted from the detector and a positive potential develops in the detector.

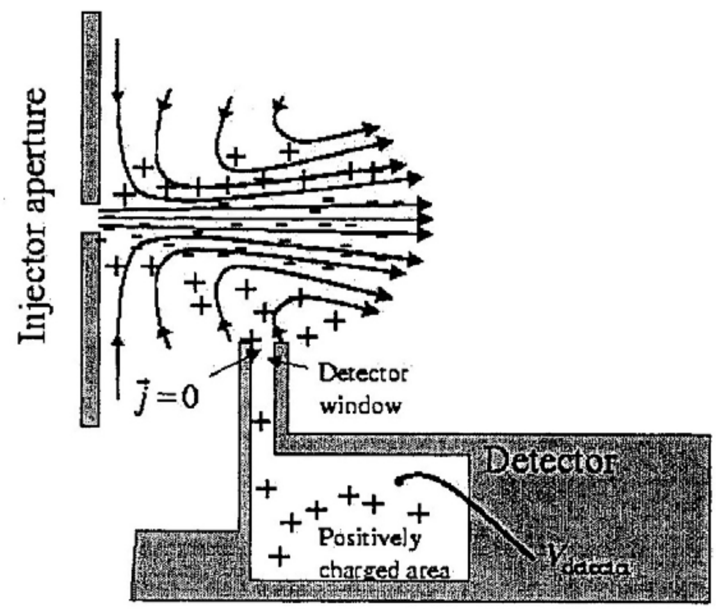

Figure 4.7: The streamlines and density distribution (schematically). The detector with window and reservoir is introduced as a probe for the potential near the main beam of electrons.

As the magnetic field is increased, the diameter of the cyclotron orbit decreases and electrons from aperture **a** will terminate in apertures **b** or **c**. This locally increases the electron density and the voltage rises rapidly at higher fields. If we continue to increase the magnetic field, the diameter of the cyclotron orbit becomes comparable to the width of the aperture and the electrons will terminate at the injecting aperture. Thus at very high magnetic fields the ballistic magnetovoltage phenomena is not observed.

We also measured the voltage at aperture **a** with respect to aperture **c** while the current was injected from aperture **b**. The same phenomenon was observed. Figure 4.8 shows that the negative peak was observed at a magnetic field B = -0.027 T. The negative sign in the magnetic field just indicates the direction of electron movement.

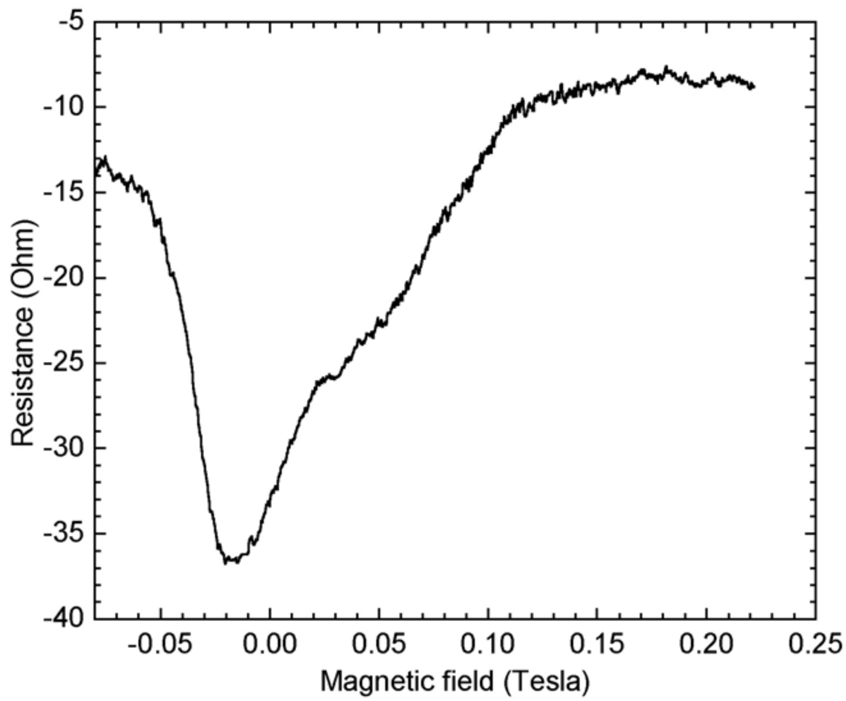

Figure 4.8: The voltage measured at aperture **a** with respect to aperture **c**, as a function of the applied perpendicular magnetic field and normalized to the current injected from aperture **b**. The gate voltage is 0.3 V and temperature is 0.4 K. The magnetic field is increased at 0.027 T/min.

In the same fashion, the voltage is measured at aperture **c** with respect to a faraway contact, as a function of the applied perpendicular magnetic field and normalized to the current injected from aperture **a**. The graph is shown in figure 4.9. The gate voltage was 0.3 V and the temperature was 0.4 K. The magnetic field was increased at 0.1 T/min.

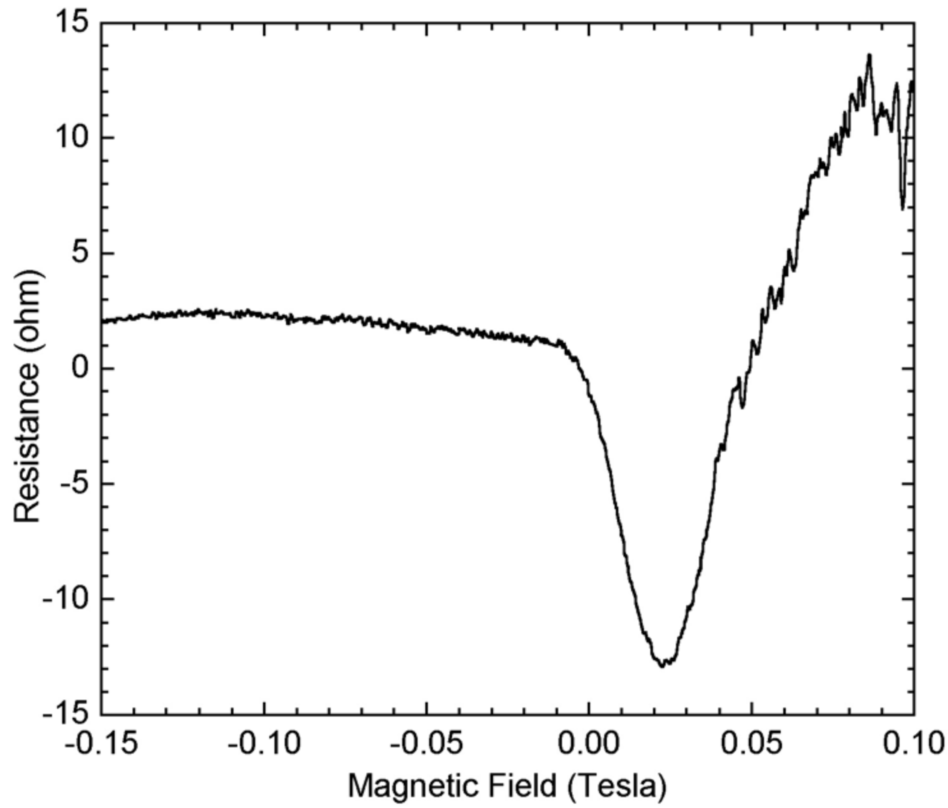

Figure 4.9: The voltage measured at aperture **c** with respect to a faraway contact, as a function of the applied perpendicular magnetic field and normalized to the current injected from aperture **a**. The gate voltage was 0.3 V and the temperature was 0.4 K. The magnetic field was decreased at 0.027 T/min.

Next, we injected current from aperture **a**. The voltage is measured at aperture **c** with respect to aperture **b**. At zero magnetic field, both apertures are at the same potential. When the magnetic field is increased, we observed a negative peak at 0.027 T as shown in figure 4.10. During the negative magnetic field sweep, we observed a negative peak at -0.027 T. The peak is not so strong because charge extraction from the aperture **b** is small.

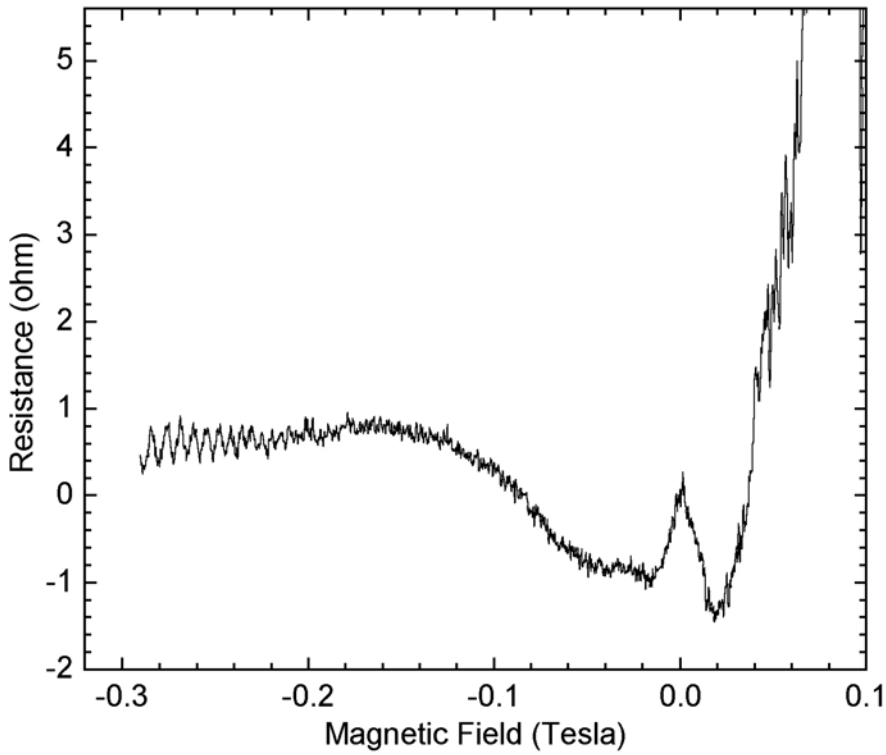

Figure 4.10: The voltage measured at aperture **c** with respect to aperture **b**, as a function of the applied perpendicular magnetic field and normalized to the current injected from aperture **a**. The gate voltage was 0.3 V and the temperature was 0.4 K. The magnetic field was decreased at 0.027 T/min.

4.2 Theory

The theoretical explanation was provided by Dr. A. O. Govorov [13]. The linearized Boltzmann transport equation is given by

$$\mathrm{v}\frac{\partial F}{\partial \mathrm{r}} - e\,\mathrm{v}E = -\frac{F - \overline{F} - 2\cos(\theta)J_x - 2\sin(\theta)J_y}{\tau_{ee}} + G(y;\theta)\delta(x) + G(y;\pi-\theta)\delta(x) \quad - (4.10)$$

where,

v is the electron velocity,

F is the density distribution function,

G(y; θ) is the injection function of current,

$$\overline{F} = \frac{1}{2\pi}\int_0^{2\pi} F(\theta)d\theta,$$

τ_{ee} is the electron-electron collision time [14], given by the equation

$$\frac{1}{\tau_{ee}} = \frac{E_F}{h}\left(\frac{KT}{E_F}\right)^2\left[\ln\left(\frac{E_F}{KT}\right)+\ln\left(\frac{4}{a_0^* k_F}\right)+1\right]$$

where, K is The Boltzmann constant, a_0^* is the effective Bohr's radius.

$$J_x = \frac{1}{2\pi}\int_0^{2\pi} F(\theta)\cos(\theta)d\theta,$$

$$J_y = \frac{1}{2\pi}\int_0^{2\pi} F(\theta)\sin(\theta)d\theta,$$

and **E** is the in-plane electric field.

For our geometry, the aperture width, w, is 0.4 μm. The number of occupied transverse channels [15] is given by

$$N = \frac{w}{\lambda_F/2} = 21.64 \approx 22 \text{ channels},$$

The conductance is

$$G_c = N\frac{2\,e^2}{h}$$

$$= \frac{22\times 2\times(1.60\times 10^{-19})^2}{6.62\times 10^{-34}}\ \text{S}$$

$$= 1.70\times 10^{-3}\ \text{S}$$

For our data analysis, this conductance does not enter in our calculations.

In the sample, the 2DES was covered with a metallic gate on the top. The sample can be treated as capacitor. When the separation between the electron gas and the gate, d, is small the potential V is proportional to the non-equilibrium density δn(r).

$$\mathbf{V} = \frac{4\,\pi\,e\,d}{\varepsilon_{sem}}\ \delta n(r) \qquad \text{---------------------------(4.11)}$$

where,

δn(r) is the non-equilibrium electron density,

ε_{sem} is the dielectric constant of the semiconductor.

So, the electric field is given by the relation

$$\mathbf{E} = \frac{4\,\pi\,e\,d}{\varepsilon_{sem}}\frac{\partial\,\delta n}{\partial\mathbf{r}} \qquad \text{--------------------(4.12)}$$

The calculations show that the non-equilibrium density is maximum at y = 0 and is negative for a small value of the y-coordinate. The magnitude of the non-equilibrium density decreases with increasing x. The non-equilibrium density gives some idea about the observed hydrodynamic pumping effect.

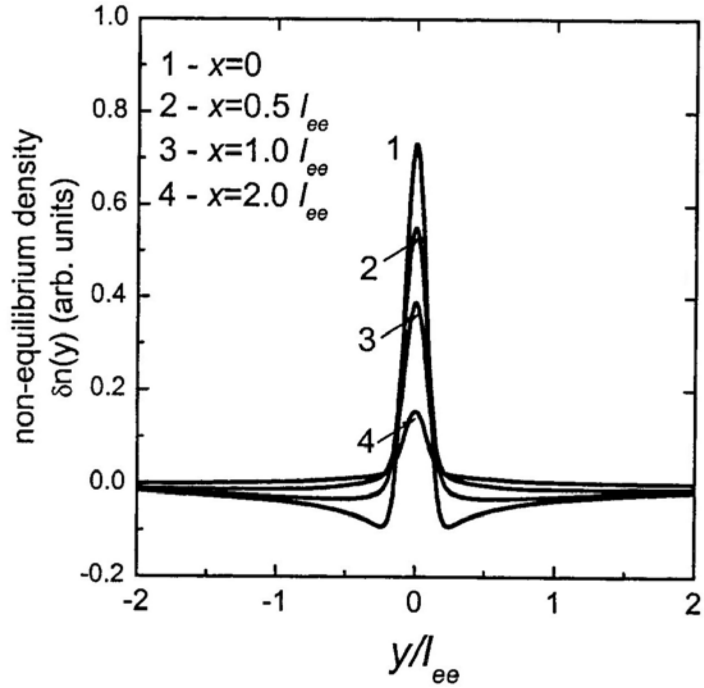

Figure 4.11: Calculated non-equilibrium density distribution as a function of the y-coordinate at several x-positions. The aperture width is assumed 0.1 l_{ee}.

4.3 Results at temperature 1.3 K

Next measurements were taken at a little higher temperature of 1.3 K and a gate voltage of 0.3 V. The sample was in a ^{4}He exchange gas. Figure 4.14 shows Shubnikov-de Haas effect when the longitudinal voltage measured between two adjacent contacts of the Hall bar is plotted as a function of inverse of applied magnetic field. The magnetic field sweeping rate was 0.1 T/min.

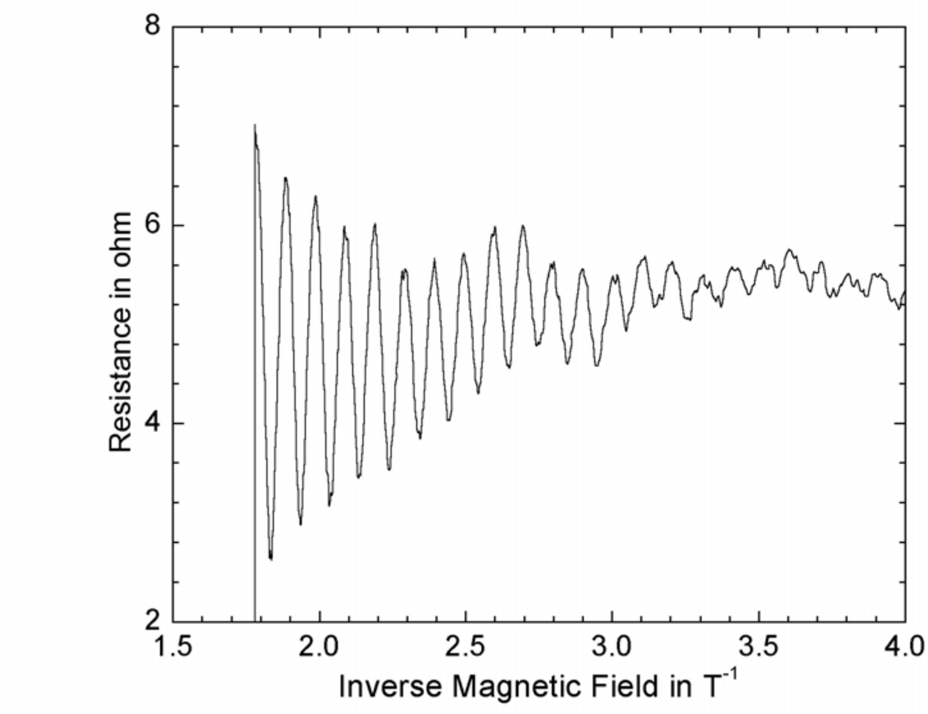

Figure 4.12: Longitudinal resistance R_L versus applied perpendicular magnetic field B_{ext} shows Shubnikov-de Haas oscillations at a temperature of 1.3 K and 0.3 V gate voltage in a uniform magnetic field sweeping at a rate 0.1 T/min.

Calculation for density of electron:

Number of periods = 10

Inverse magnetic Field = $1\mathrm{T}^{-1}$

Period of oscillations $T = \dfrac{\text{Inverse Magnetic Field}}{\text{No.of periods}} = \dfrac{1}{10}\ \mathrm{T}^{-1}$

Frequency $f = \dfrac{1}{T} = 10\mathrm{T}$

Density of electrons, $n = 4.84 \times 10^{10}\ \mathrm{cm}^{-2}\ \mathrm{T}^{-1} \times f$

$= 4.84 \times 10^{10} \times 10\ \mathrm{cm}^{-2}$

$= 4.84 \times 10^{11}\ \mathrm{cm}^{-2}$

$$= 4.84 \times 10^{11}\ \mathrm{m}^{-2}$$

Figure 4.13 shows the transverse voltage measured across the Hall bar as a function of the applied perpendicular magnetic field. The transverse voltage is divided by the applied current to obtain the transresistance. The applied current is set at 100 nA. The slope of the line gives the Hall coefficient.

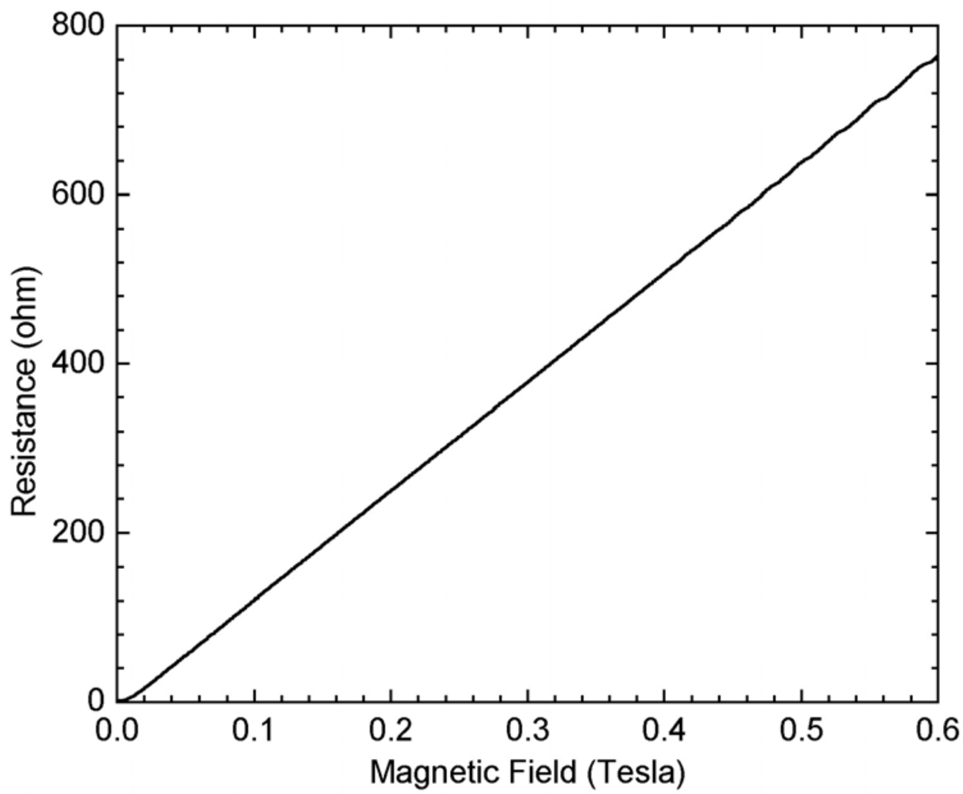

Figure 4.13: The transverse Resistance R as a function of the applied perpendicular magnetic field at a temperature of 1.3 K and 0.3 V gate voltage.

From the graph,

Hall coefficient = Slope of straight line plotted resistance vs. the magnetic field

$$= 1290.52\ \Omega/\mathrm{T}$$

From equation (3.4),

$$\text{Hall Coefficient } R_h = -\frac{1}{n\,e}$$

$$\text{or, } n = -\frac{1}{e\,R_h}$$

$$= \frac{1}{1.6\times10^{-19}\times1290.52}\ \text{m}^{-2}$$

$$= 4.84\times10^{15}\ \text{m}^{-2}$$

Longitudinal voltage V = 2.01 × 10^{-6} V

Applied current I = 100 × 10^{-9} A

$$\text{Resistance } R = \frac{V}{I} = \frac{2.01\times10^{-6}}{100\times10^{-9}} = 20.1\ \Omega$$

Resistivity is given by

$$\rho = \frac{\text{w}}{\text{L}} R = \frac{150}{300}\times20.1 = 10.05\ \Omega$$

$$\text{Mobility } \mu = \frac{1}{ne\rho}$$

$$= \frac{1}{4.84\times10^{15}\times1.60\times10^{-19}\times10.05}\ \text{m}^2/\text{Vs}$$

$$= 128\ \text{m}^2/\text{Vs}$$

$$\text{Mean Free Path, } l_\mu = \frac{\hbar}{e}\sqrt{2\pi}\,\mu\sqrt{n}$$

$$= \frac{1.05\times10^{-34}\times\sqrt{2\times3.14}\times128\times\sqrt{4.84\times10^{15}}}{1.60\times10^{-19}}\ \text{m}$$

$= 14.6 \times 10^{-6}$ m

$= 14.6$ μm

The Fermi wave vector K_F in the 2D system in terms of the density of electrons **n** is

$$K_F = (2\pi\,\mathbf{n})^{1/2}$$

$$= (2\times3.14\times4.84\times10^{15})^{1/2}\ \text{m}^{-1}$$

$= 1.74 \times 10^{8}$ m^{-1}

The Fermi energy of the system is

$$E_F = \frac{\hbar^2 K_F^2}{2m}$$

$$= \frac{(1.05\times10^{-34})^2\times(1.74\times10^{8})^2}{2\times0.067\times9.11\times10^{-31}}\ \text{J}$$

$= 2.74 \times 10^{-21}$ J

$= 17.16$ meV

The Fermi wavelength is

$$\lambda_F = \frac{2\pi}{K_F} = 3.61 \times 10^{-8}\ \text{m}$$

The Fermi velocity is

$$mV_F = \hbar K_F$$

$$\text{or, } V_f = \frac{1.05\times10^{-34}\times1.74\times10^{8}}{0.067\times9.11\times10^{-31}}\ \text{m/s}$$

or, $V_F = 2.99 \times 10^{5}$ m/s

In this case, we performed current measurements at a temperature of 1.3 K. An AC signal of 100 nA was applied from the aperture **a** and the current was measured at the aperture **b**. Both apertures were referenced to some faraway contact. The lock-in amplifier was used to source the current. The output signal was measured through a low noise current preamplifier. The graph is shown in figure 4.14.

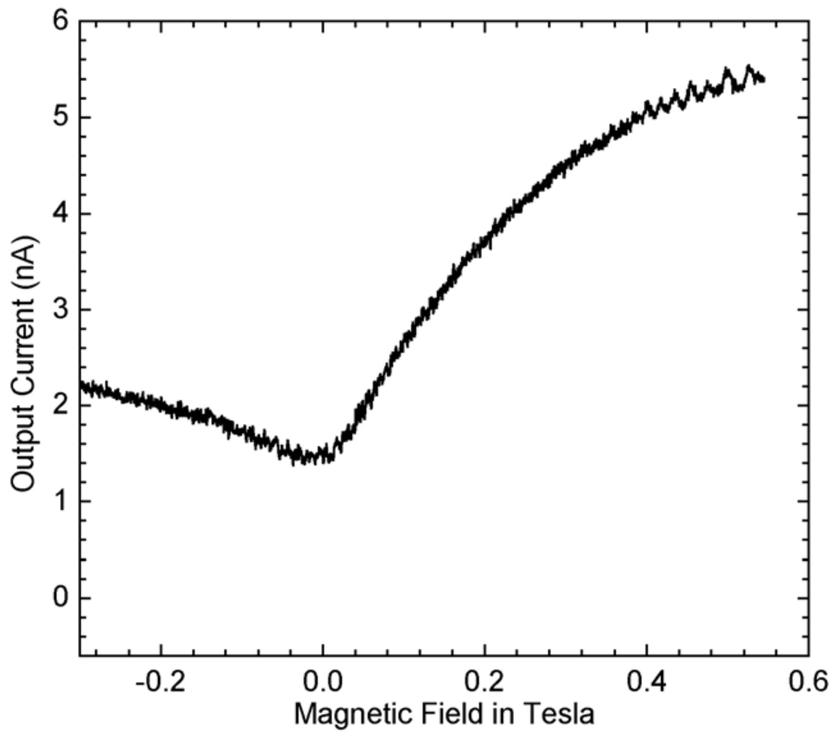

Figure 4.14: The extracted current at aperture **b** with respect to faraway contact as a function of the applied perpendicular magnetic field. An AC signal of 100 nA is injected from aperture **a** at a temperature of 1.3 K and a gate voltage of 0.3 V. The output signal is measured through a low noise current preamplifier.

The current measurements were repeated, this time with an AC signal of 100 nA applied at the aperture **a** with respect to faraway contact and the output current was measured at aperture **b** using the lock-in amplifier. The same effect was observed. In comparison to the voltage measurement, the output signal was more noisy.

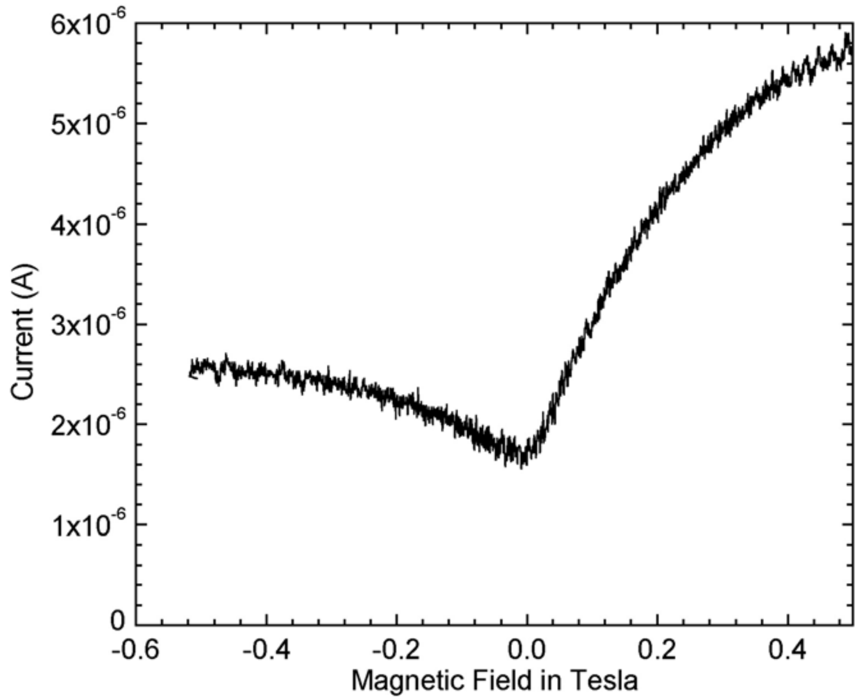

Figure 4.15: The extracted current at aperture **b** with respect to faraway contact as a function of the applied perpendicular magnetic field. An AC current of 100 nA is injected from aperture **a** at a temperature of 1.3 K and a gate voltage of 0.3 V. The output signal is measured through a lock-in amplifier.

We also performed some dc current measurements. The dc current was injected from the aperture **a** through a current source. The output current was measured at the aperture **b** using a low noise current preamplifier. The magnetic field was swept up at a rate of 0.05 T/min.

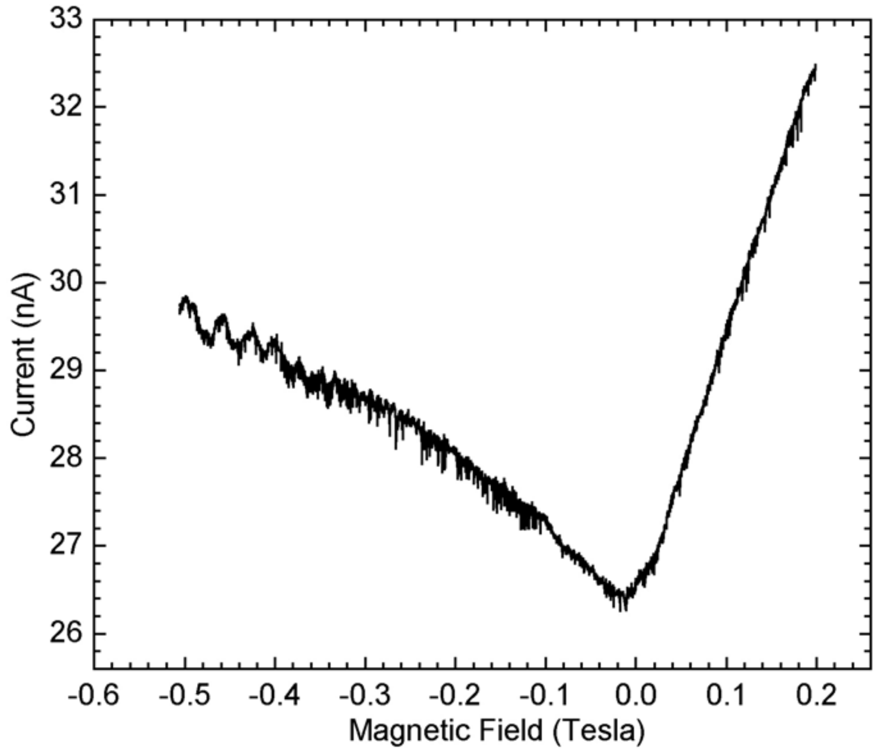

Figure 4.16: The extracted current at aperture **b** with respect to a faraway contact as a function of the applied perpendicular magnetic field. A DC signal of 100 nA is injected from aperture **a** at a temperature of 1.3 K and a gate voltage of 0.3 V.

Our measurements confirmed that current could be extracted or induced through aperture **b** for both DC current and AC current fed through aperture **a** at T=1.3 K. One experiment was done to verify the linearity relationship between the injected current and the extracted current. There were complications in the experimental setup for the measurement of nanoampere currents. This small signal might be offset by few nanoamperes due to thermal electromotive force developed at connection terminals. So an excitation current for the range of –5 μA to 5 μA was injected from the aperture **a**, and the extracted current was measured at the aperture b. The result is shown in figure 4.17. The straight line passes through the origin. From the graph, it is evident that the pumping force changes direction when the current is reversed. This phenomenon is qualitatively different from the Bernoulli effect, where the pumping force is quadratic in terms of the fluid speed and there is no change in direction with a change in direction of the current. No deviations from linearity were observed over current biases of ±5 μA.

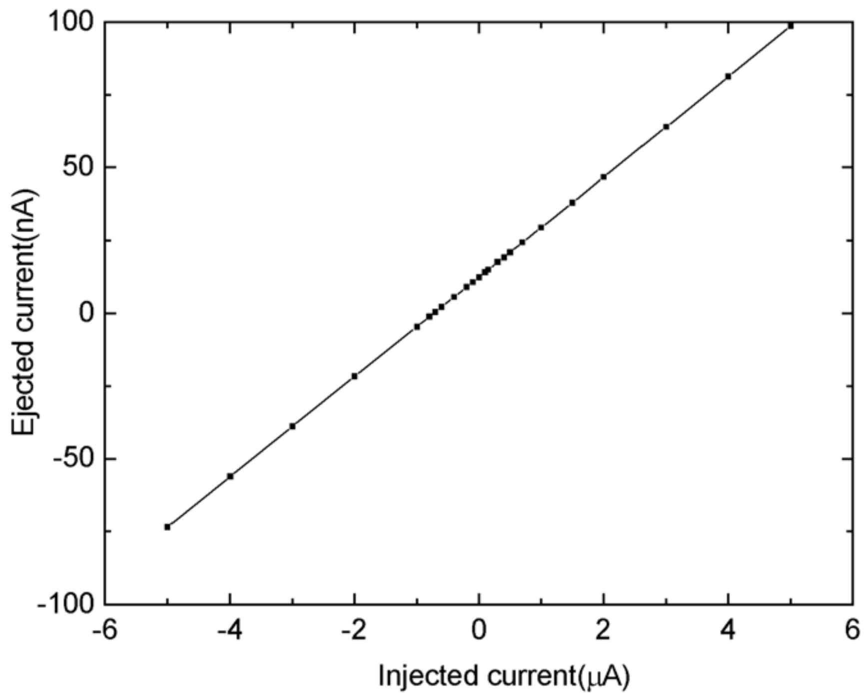

Figure 4.17: Linear dependence of the current measured through aperture **b** as a function of the current injected from aperture **a**, in DC mode. A current offset is present due to the voltage bias of aperture **b**.

4.4 Temperature Dependence

We also observed the effect of temperature on the hydrodynamic pumping. In high mobility 2DES at low temperatures, the electron-electron interaction path l_{ee} can be longer than the momentum relaxation path l_{μ}. The electron-electron collision time τ_{ee} [14] is given by

$$\frac{1}{\tau_{ee}} = \frac{E_F}{h}\left(\frac{KT}{E_F}\right)^2\left[\ln\left(\frac{E_F}{KT}\right) + \ln\left(\frac{4}{a_0^* k_F}\right) + 1\right]$$

The electron-electron interaction path is

$$l_{ee} = V_f \tau_{ee}$$

where V_f is Fermi velocity.

In our case at temperature T = 1.23 K and the density of electrons, n = 4.84 × 10^{15} m^{-2},

l_μ = 14.6 μm

τ_{ee} = 911.98 × 10^{-12} sec

l_{ee} = 273.58 μm

In our theoretical explanation for the observed hydrodynamic effect, we only considered the case where the momentum relaxation mean free path is larger than the electron-electron interaction path. So in the lower temperature limit our theory fails to explain the observed phenomenon.

We found that the density of electrons is constant with respect to temperature. But the mobility of electrons is strongly dependent on temperature as shown in figure 4.18.

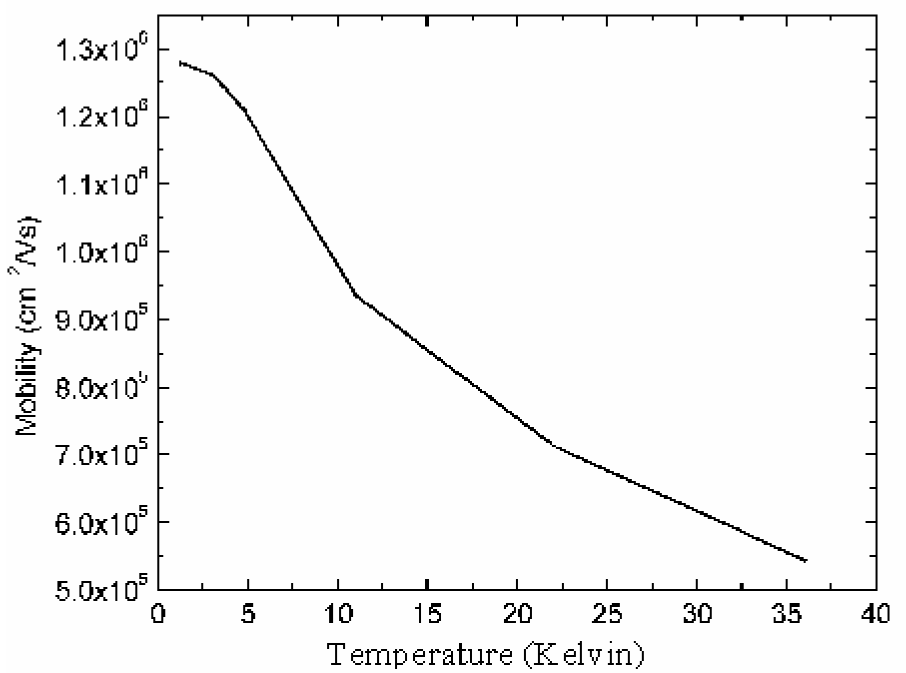

Figure 4.18: The mobility of charge carriers as a function of temperature. The density of electrons is approximately constant with temperature.

At higher temperatures, the mean free path also decreases. As a result of this the electron-electron interaction path and the momentum relaxation mean free path become comparable to the device dimensions.

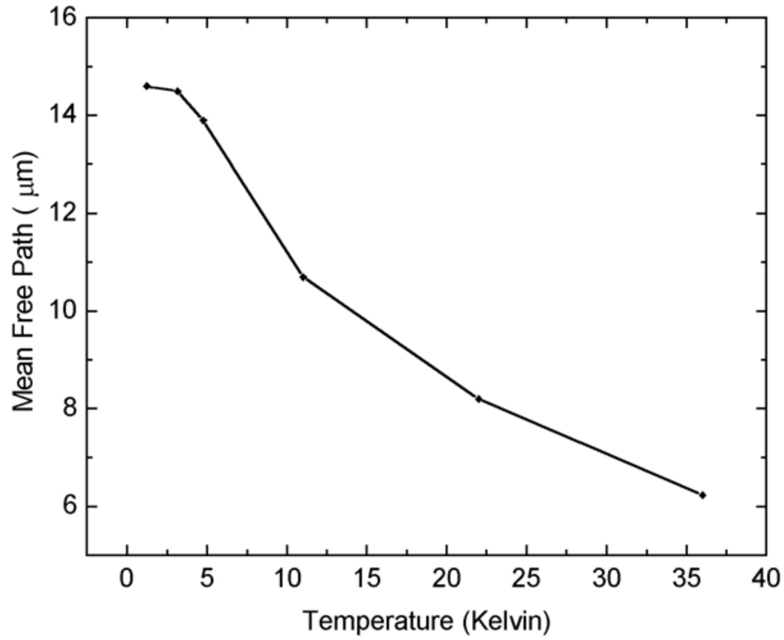

Figure 4.19: The mean free path as a function of temperature. The square symbol denotes data points.

Experiments were also carried out at different temperatures of 1.23 K, 3.14 K, 4.45 K, 11.10 K, 22 K and 36 K. Figure 4.20 shows all the curves at these different temperatures. We observed that the hydrodynamic pumping was stronger in the lower temperature regime (T = 0.33 K to 4.45 K). In the higher temperature limit, the hydrodynamic pumping is not so strong. At T = 36 K, the negative peak disappears.

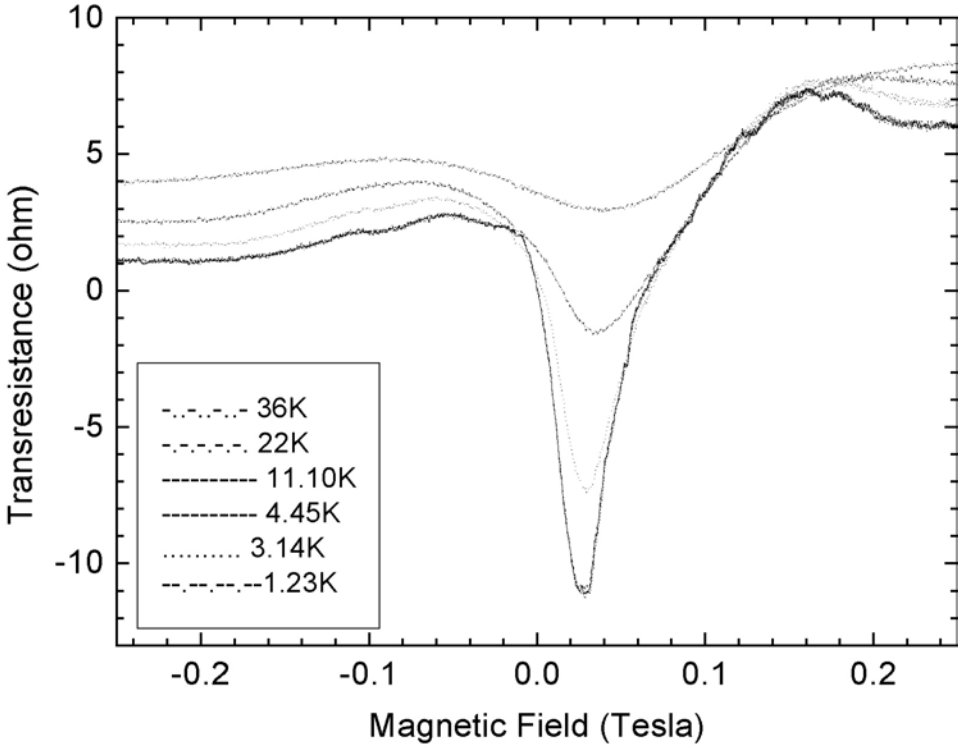

Figure 4.20: The transresistance of the sample at aperture **b** as a function of the magnetic field at different temperatures. An AC current of 100 nA is applied at aperture **a** and a voltage is measured at aperture **b**.

Conclusion

We studied the hydrodynamic pumping effect at low temperatures as well as the temperature dependence of this effect. All our measurements showed that the pumping force is linear in terms of the applied voltage. At low temperatures, the electron-electron interaction is very weak in the Fermi liquid. Electrons obey Fermi statistics. We conclude that the ejected current at one aperture is directly proportional to the injected current from another aperture.

The hydrodynamic pumping depends on temperature. At lower temperatures, the electron-electron interaction path and the momentum relaxation mean free path far exceeds the device dimensions. This is one of the most essential conditions for this pumping effect. The electron-electron collision time is larger at low temperatures. It leads to a weak electron-electron interaction.

As temperature increases, the collision time decreases and the electron-electron interaction becomes stronger. The electron-electron interaction path l_{ee} becomes comparable to or even less than the device dimension. Also the extraction of charge carriers from the detector decreases. At a temperature of T = 36 K, we observed that there was no negative potential at aperture **b**.

All experiments were performed on a single geometry. The other feature such as small peak at magnetic field B = 0.05 T are unexplained. Further experimental results will be helpful in explaining hydrodynamic pumping effect more clearly. The optimization of device geometry can be taken into account for future work. Some results of this experiment will be published as " Hydrodynamic pumping effect of a quantum

Fermi liquid in a semiconductor heterostructure" by J. J. Heremans, A.O. Govorov, D. Kantha and Z. Nikodijevic.

Bibliography

1. Reymond A. Serway, Jerry S. Faughn, *College Physics*, Second Edition,Saunders College Publishing.
2. R. Byron Bird, Warren E. Stewart, Edwin N. Lightfoot, *Transport Phenomena*, John Wiley & Sons.
3. M.J.M. de Jong and L.W. Molenkamp, *Hydrodynamic electron flow in high mobility wires,* Phys. Rev. B **51**, 13389.
4. H.Predel, H.Buhmann, L.W. Molenkamp, R.N. Gurzhi, A.N. kalinenko, A.I. Kopeliovich and A.V. Yanovsky, *Effects of electron-electron scattering on electron-beam propagation in a two-dimensional electron gas,* Physics Review B **62**, 2057 (2000).
5. J.J. Heremans, S. von Molnar, D.D. Awschalom and A.C. Gossard, *Ballistic electron focusing by elliptic reflecting barriers,* Applied Physics Letter **74**, 1281(1999).
6. J.J. Heremans, M.B. Santos and M. Shayegan, *Observation of magnetic focusing in two-dimensional hole systems,* Applied Physics Letter **61**, 1652 (1992).
7. Y. Hirayama, T. Saku, S. Tarucha and Y. Horikoshi, *Ballistic electron transport in macroscopic four terminal square structures with high mobility,* Applied. Physics Letter **58**, 2672(1991).
8. http://www.ece.gatech.edu/research/labs/vc/theory/photolith.htm.
9. Mark A. McCord, Michael J. Rooks, *Handbook of Microlithography, Micromachining and Microfabrication*,

(http:// www.nnf.cornell.edu/SPIEBook/TOC.HTM).

10. Donald M. Munroe, *A lock-in Amplifier Primer*, Princeton Applied Research Corp, Princeton.
11. John H. Davies, *The Physics of Low Dimensional Semiconductors*, First Edition, Cambridge University Press.
12. Charles Kittel, *Introduction to Solid State Physics*, Sixth Edition, John Wiley and Sons, Inc.
13. A. O. Govorov et al., unpublished.
14. G.F. Giuliani and J.J. Quinn, *Lifetime of a quasiparticle in a two-dimensional electron gas*, Physics Review B **26**, 4421(1982).
15. B. J. van Wees, H. van Houten, C. W. J. Beenakker, J. G. Williamson, L. P. Kouwenhoven, D. van der Marel and C. T. Foxen, *Quantized Conductance of Point Contacts in a Two-Dimensional Electron Gas,* Physics Review Letter **60**, 848 (1998)